SAND2017-9385C

# High Power-Density Photovoltaic Boost Converter and Inverter Using GaN and AlGaN Devices Housed in 3D Printed Packages

Robert Brocato
Sandia National Laboratories
Albuquerque, USA
(contact email: rwbroca@sandia.gov)

***Abstract*— A power converter capable of converting the 48 V DC output of a photovoltaic panel into 120 V AC at up to 400 W has been demonstrated in a 40 cu. cm. (2.4 cu. in.) module, for a power density of greater than 160 W/cu. in. The module is enabled by the use of GaN and AlGaN field effect transistors (FETs) and diodes operating at higher power densities and higher switching frequencies than conventional silicon power devices. Typical photovoltaic panel converter/inverters have power densities ranging from 3.5-5.0 W/cu. in. and often make use of bulky, low frequency transformers. By using wide- and ultra-wide-bandgap switching devices, the operating frequency has been increased to 150 kHz, eliminating the need to use low frequency charge and current storage elements. The resulting size reduction demonstrates the significant possibilities that the adoption of GaN and AlGaN devices housed in small, 3D printed packages offers in the field of power electronics.**

***Keywords—GaN; AlGaN; power conversion; inverter; photovoltaic***

## I. INTRODUCTION

Increasing demand for electrical energy globally is leading to a rapid increase in the capacity of installed solar photovoltaic based electrical generation. Some are projecting that solar-generated power will dominate new energy generation within as little as 12 years [1]. As solar generation expands, it is projected to be used in many isolated locations for new applications to meet critical future food, energy, and water needs [2]. These isolated locations may make use of multiple different electrical energy sources combined into a microgrid or otherwise operating in a decentralized manner [3]. To accommodate these various applications, a small, flexible conversion device is needed to be able to serve as an interface between the solar photovoltaic array output and the next input. The next input might consist of a conventional electrical grid, an AC-powered consumer device, or a local microgrid that may include a distributed array of panels, other renewable energy devices, and storage devices.

To accomplish this, a boost converter/inverter power module can be used. The task of the small-sized boost converter/inverter is to turn the 48 V DC output of a standard photovoltaic array into a 120 V, 50/60 Hz AC signal capable of providing power for consumer use or grid connection. Larger sized power converters will often have a 240 V AC output. Boost converters/inverters capable of doing this are available from a number of different commercial suppliers. Our motivation with this project has been to greatly reduce the size and weight of the device by increasing the operating frequency. Increasing the operating frequency leads to a decrease in the size of the current and charge storage elements. Ultimately, this should also lead to a substantial decrease in cost, since the current and charge storage elements are primary cost drivers of power converters.

Our power converter was created as an exemplar circuit to demonstrate the potential for reducing size and weight of a boost converter/inverter by using GaN and AlGaN power devices in custom 3D printed electronic packages. The GaN, AlGaN devices, and the custom 3D printed electronic packages were created as part of the Ultra-Wide-Band-Gap (UWBG) Grand Challenge Laboratory-Directed Research and Development (GC-LDRD) Project at Sandia National Laboratories. The wide bandgaps of GaN and AlGaN allow for improvements over conventional Si devices in several areas. First, voltage hold-off improves with increasing bandgap, since the critical field scales with bandgap. The bandgaps of GaN (3.2 eV) and AlGaN (4.2-6.3 eV) are significantly wider than that of Si (1.12 eV). Second, high temperature operation improves with increasing bandgap, since the number of free carriers decreases significantly with increasing bandgap [4]. The wide-bandgap provides low intrinsic carrier concentration according to the familiar exponential relation of the law of mass action:

$$np = n_i^2 = N_C N_V e^{-E_G/kT} \quad (1)$$

where $n_i$ is the intrinsic carrier concentration, n is the electron

concentration, p is the hole concentration, $N_C$ is the conduction band density of states, $N_V$ is the valence band density of states, $E_G$ is the bandgap, k is Boltzmann's constant, and T is the temperature. From Eqn. 1, it can be seen that a wider bandgap will need a higher operating temperature to achieve a given carrier concentration. Consequently, wide- and ultra-wide-bandgap semiconductors are capable of operating at higher temperatures than silicon power devices. Finally, semiconductor high frequency operation improves with increasing bandgap, as physical size and its accompanying parasitic capacitance decrease [5].

## II. Design Overview

### A. Converter Architecture

GaN and AlGaN diodes and FETs have been successfully fabricated at Sandia as part of the UWBG GC-LDRD Project. Due to a lack of suitable, commercially-available, high-power-handling, small footprint electronic packages, a family of high-voltage electronic packages was created. These were created both to accommodate the new power devices and other, commercially available power devices, as they become available (Fig. 1). The packages were created to accommodate both single devices, serial-, and parallel-connected devices (Fig. 2). A test regime was developed to characterize package and device performance separately and together [6]. To demonstrate the capabilities of the packaged GaN and AlGaN devices, a prototype power converter module was created (Fig. 3). The converter module operates by stepping the 20-60 V DC output of a typical photovoltaic module up to 250 V DC then inverting the DC output to produce the 120 V AC output.

The circuit makes use of analog-tuned sub-circuits to enable creation of a super-compact, low cost module. It consists of three main blocks (Fig. 4). These blocks are as follows: (1) a 15 V linear regulator to power board circuitry, (2) a 48 V DC to 250 V DC boost converter, and (3) a 250 V DC to 120 V AC inverter. The linear regulator is powered directly from the raw DC input power line and typically supplies 60-80 mA of current at 15 V to power the boost converter and inverter circuitry. The boost converter is also supplied from the raw DC input power line. The boost converter is used to turn the 20-60 V input into a 250 V regulated DC output. The boost converter operates at 150 kHz switching frequency by using a commercially available GaN FET in a standard surface-mount package and four paralleled GaN diodes packaged in a custom 3D printed package. The 250 V DC output is converted by the inverter into 120 V, 60 Hz. AC, suitable for grid connection or direct consumer application. Like the boost converter section, the inverter section also operates at 150 kHz. It uses both commercially available GaN devices and custom GaN and AlGaN devices housed in custom 3D printed packages. The board includes both a 60 Hz reference oscillator and the ability to accept and synchronize to an externally supplied 60 Hz input. This enables either stand-alone or grid–connected operation.

### B. Circuit Implementation

A detailed block diagram of the circuit is shown in Fig. 5. The linear regulator supplies the other circuitry on the board, and its 15 V output initiates the primary power switching circuitry. There are two oscillators used to establish timing on the board, the 60 Hz and 150 kHz oscillators. Both use CMOS logic operating at 15 V. Both oscillators need to have duty factors very close to 50% in order for follow-on circuitry to operate correctly. The 60 Hz oscillator can be over-ridden by an externally-supplied 50-60 Hz signal, typically coming from an active grid. If the grid-supplied 50-60 Hz signal fails or is disconnected, the internal 60 Hz oscillator supplies the frequency reference.

Immediately following both oscillators are sawtooth converters which turn the input square-waves into symmetrical sawtooth waves at the oscillator frequency. The sawtooth converters consist of an op-amp-based feedforward integrator with a time constant set to slightly faster than the input frequency and a second op-amp integrator with a much longer time constant to provide level adjusting feedback to the feedforward integrator. There are three of these sawtooth converters, one for the 60 Hz signal, and two for the 150 kHz signal. The 60 Hz sawtooth signal provides a reference signal for a pair of window-detecting comparators that follow the sawtooth converters. The second input to each of the comparators is the output of either of the two 150 kHz sawtooth converters. The outputs of the two 150 kHz sawtooth converters are set to occupy the upper portion of the 60 Hz sawtooth signal, for one, and the lower portion of the 60 Hz sawtooth signal, for the other. The combination of the sawtooth converters and the comparators provides a pair of 60 Hz signals that are pulse-width modulated at 150 kHz (Fig. 5).

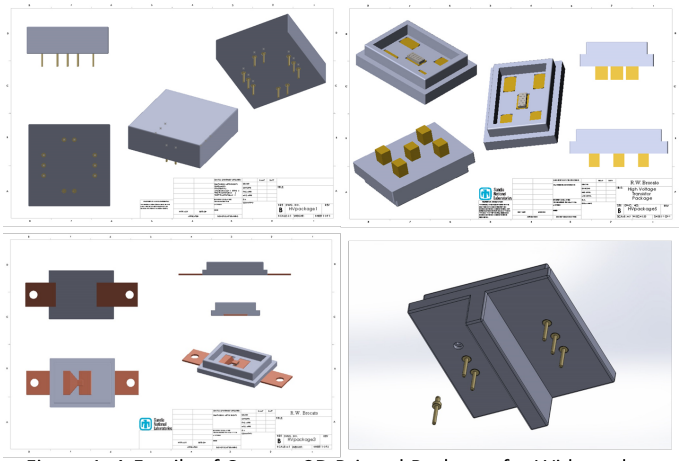

Figure 1: A Family of Custom 3D Printed Packages for Wide and Ultra-wide Bandgap Semiconductors in Various Applications.

### C. Tying to the Grid

As mentioned, the module can operate either in stand-alone or grid-connected mode. If an external grid connection is made, the circuit senses the presence of a 50-60 Hz input and automatically switches out its own internal 60 Hz reference

oscillator. In this way, the output of the board is synchronized to the grid, if a grid connection is available. If it is desired to create a microgrid from an array of these boards, it is possible to operate one board as the frequency reference, and the other boards can be operated synchronized to that source.

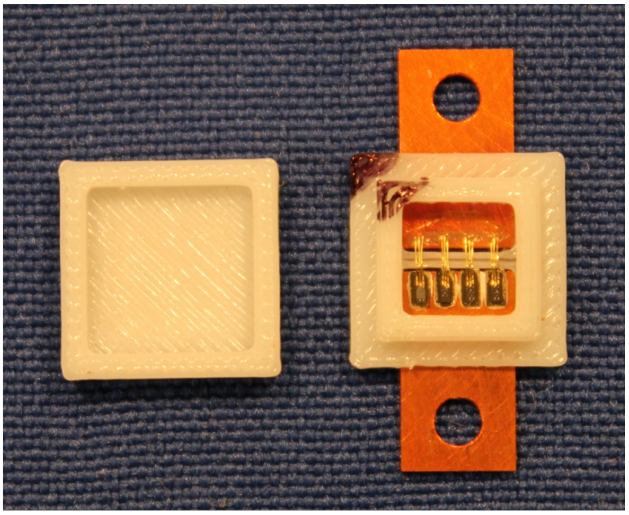

Figure 2: Parallel GaN Diodes in Custom 3D Printed Package

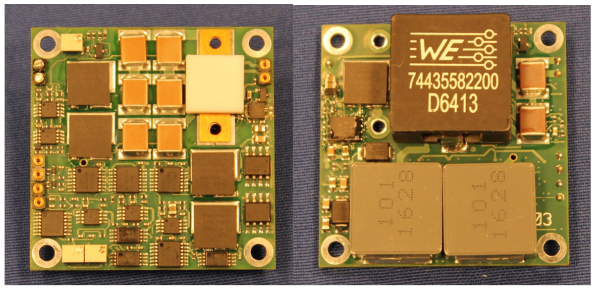


Figure 3: Front and Back Views of the Voltage Converter/ Inverter Module

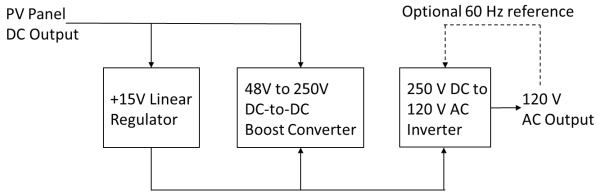


Figure 4: Boost Converter/ Inverter Block Diagram

## III. PACKAGING

### A. Overview

We initially overlooked the special needs of electronic packaging that we would encounter in developing power GaN and AlGaN devices. We assumed that commercially available products would meet our needs. However, we soon learned that there were no commercially available electronic packages for high voltage and high speed operation in small physical footprints. To meet these requirements, we developed design, fabrication, and test capabilities for prototype electronic packaging with a special emphasis on high voltage breakdown testing [6]. We then developed a family of different electronic packages for different devices and applications.

### B. Low Budget 3D Printing of Electronic Packages

In order to be able to quickly develop usable products, we made use of 3D printing. Our capabilities mostly consist of commercially available 3D printers which print a variety of different plastics. We combined this capability, in some cases, with custom machined metal pins, and in other cases, with commercially available metal pins. We designed these combinations using commercially available mechanical CAD tools. We used a standard 1-ton press to fit the pins into the package shells. We used a standard ribbon wire-bonder using 3x0.5 mil gold ribbon wire to create electrical connections from the electronic components to the pins within the packages. Using these methods, we were able to create electronic packages capable of operating at high voltages but with the same size footprint as common low voltage packages.

We found that tolerances on the 3D printed plastic shells were sufficiently tight, that we could use press-fitting for all of the pins into the shells. The pins do not fall out through subsequent wire-bonding, testing, and pcb connecting operations. This occurs in spite of the fact that the 3D printed package shells that we produced are somewhat less rugged than commercial plastic package shells. The resulting electronic packages are suitable for prototyping or small scale production, but are probably not well suited to high volume production applications.

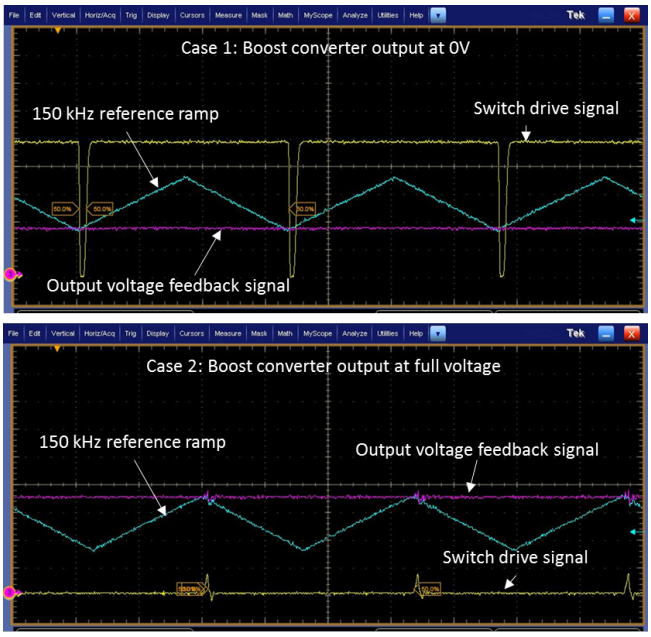


Figure 6: Boost converter control signals.

## IV. Test Results

### A. Overview

The Sandia-fabricated GaN and AlGaN diodes that were created as part of the UWBG GC-LDRD project were tested both as die and in their 3D printed packages [6]. After component-level testing, these devices were inserted into the power converter shown in Fig. 3. The power converter was then tested as a stand-alone module.

### B. Boost Converter

The boost converter uses a single inductor paired with a GaN FET and the GaN diode shown in figure 2. Its output level is controlled by a pulse-width modulated control loop operating at 150 kHz. We found that optimum operation of the boost converter was the most important element to correct operation of the entire module. The two input signals to the boost converter comparator, shown in Fig. 5, along with the one output signal are shown as oscilloscope traces in Fig. 6. The top of the figure shows the boost converter control signals at startup. The 150 kHz ramp signal (Fig. 6: green trace) is compared to the voltage feedback signal (Fig. 6: red trace). The comparator output (Fig. 6: yellow trace) is then used to drive the boost converter switch.

The bottom of Fig. 6 shows the boost converter control signals with the output of the boost converter at full voltage under a lightly loaded condition. For this case, the output feedback signal (Fig. 6: red trace) is at the top of the range established by the 150 kHz ramp signal (Fig. 6: green trace). The comparator output (Fig. 6: yellow trace) shows that only a very narrow pulse is needed to drive the converter switch. To adjust the boost converter output, the ratio of the feedback resistive divider can be changed to set the voltage level. Also, the feedback divider amplifier gain can be adjusted to change the sensitivity of the controller to the output load value. For our testing, the output of the boost converter was set to 250-300 V DC.

### C. Inverter

The inverter follows the boost converter and receives its input from the DC voltage output of the boost converter. The inverter has similar control circuitry to that of the boost converter. That is, the 150 kHz oscillator is used to produce a pair of sawtooth signals that are used to create a pair of sinusoidally varying pulse-width modulated signals. One sawtooth signal occupies the upper half of the voltage comparison window, and the other sawtooth signal occupies the lower half. The voltage levels of the voltage comparison window are established by a third sawtooth signal operating at 60 Hz, or at the connected grid operating frequency. The two 150 kHz sawtooth signals are compared against the 60 Hz sawtooth signal to produce the pair of sinusoidally varying pulse-width modulated control signals.

These control signals are used to drive a full bridge created from the cross-connection of four GaN FETs. One of the pulse-width modulated control signals is used to create the upper half of the desired sine-wave output, while the other control signal is used to create the lower half (Fig. 5). The pulse-width modulated control signals drive alternate paths through the load via the bridge. The differential bridge output is filtered via differential LC low-pass filters. These filters remove the 150 kHz component and leave the 60 Hz component. Oscilloscope traces of the pulse-width modulated control signals, along with the resulting AC output signal with no attached load, are shown in Fig. 7.

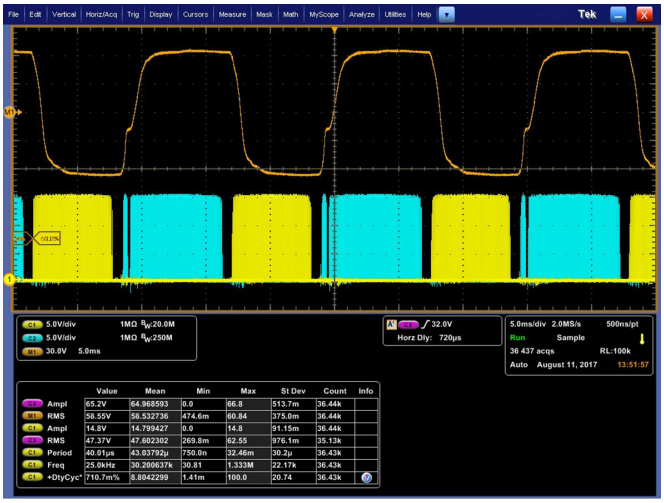


Figure 7: AC Output with Bridge Input Drive Signals

### D. Module Testing

As of this writing, testing of the boost converter/inverter module is not yet fully completed. Thus far, we have completed functional testing of the module at moderate loads. We still need to complete testing of the module for efficiency at a full load of 400W.

## V. Conclusion and Follow-On Work

We have successfully demonstrated the advantages of using wide- and ultra-wide-bandgap devices in power conversion applications for reducing size and weight of converter modules. We believe that the advantage of lower price will in time also be able to be included in this list, due to the smaller size inductors and capacitors that are needed for operation in these applications. While solar photovoltaic applications are often not tightly space or weight constrained, there are advantages to including a small boost converter/inverter with each photovoltaic panel. This approach affords degraded operation, rather than complete failure, in the event of module failure on a single panel.

As a follow-on effort, creation of a GaN and AlGaN enabled buck-converter for microsystem-enabled photovoltaic (MEPV) cells, could enable higher reliability photovoltaic systems. This could be brought about by combining the defect or localized failure limiting effects of MEPV with small

converter/inverters tied to each photovoltaic panel [7] [8]. The resulting combination could enable degraded operation, rather than system failure, in the event of single panel failure.

## ACKNOWLEDGMENT

This work was supported by Sandia National Laboratories. Sandia National Laboratories is a multimission laboratory managed and operated by National Technology and Engineering Solutions of Sandia, LLC, a wholly owned subsidiary of Honeywell International, Inc., for the U.S. Department of Energy's National Nuclear Security Administration under contract DE-NA-0003525.

## REFERENCES

[1] D.Z. Morris, "Ray Kurzweil: Here's Why Solar Will Dominate Energy Within 12 Years," *Fortune Magazine,* Apr. 16, 2016.

[2] E. Gencer, C. Miskin, X. Sun, M.R. Khan, P. Bermel, M.A. Alam, and R. Agrawal, "Directing Solar Photons to Sustainably Meet Food, Energy, and Water Needs," *Nature: Scientific Reports,* 7:3133, Jun. 9, 2017.

[3] N. Hatziargyiou, H. Asano, R. Iravani, and C. Marnay, "Microgrids: An Overview of Ongoing Research, Development, and Demonstration Projects," *IEEE Power and Energy Magazine,* pp. 78-94, Jul./Aug. 2007.

[4] T.P. Chow and R. Tyagi, "Wide Bandgap Compound Semiconductors for Superior High-Voltage Unipolar Power Devices", *IEEE Trans. Elect. Dev.,* vol. 41, no. 8, pp. 1481-1483, 1994.

[5] J. L. Hudgins, G.S. Simin, E.Santi, M.A. Khan, "An Assessment of Wide Bandgap Semiconductors for Power Devices," *IEEE Trans. Power Electron.*, vol. 18, no. 3, pp. 907-914, 2003.

[6] L.J. Rashkin, R.W. Brocato, J.J. Delhotal, J.C. Neely, J.D. Flicker, L. Fang, and R.J. Kaplar, "Miniature High Voltage, High Temperature Component Package Development," *2016 IEEE Power Mod. and High Volt. Conf.*, San Francisco, Jul. 06-09, 2016.

[7] G.N. Nielson, M. Okandan, J.L. Cruz-Campa, P.J. Resnick, M.W. Wanlass, P.J. Clews, T.C. Pluym, C.A. Sanchez, V.P. Gupta, "Microfabrication of Microsystem-Enabled Photovoltaic (MEPV) Cells," *Proc. SPIE MOEMS-MEMS,* San Francisco, vol. 7927, Feb. 14, 2011.

[8] B.B. Yang, J.L. Cruz-Campa, G.S. Haase, E.I. Cole Jr., P. Tangyunyong, P.J. Resnick, A.C. Kilgo, M. Okandan, G.N Nielson, "Failure Analysis Techniques for Microsystems-Enabled Photovoltaics", *IEEE Jour. of Photovoltaics,* vol. 4, no. 1, pp. 470-476, Jan. 2014.

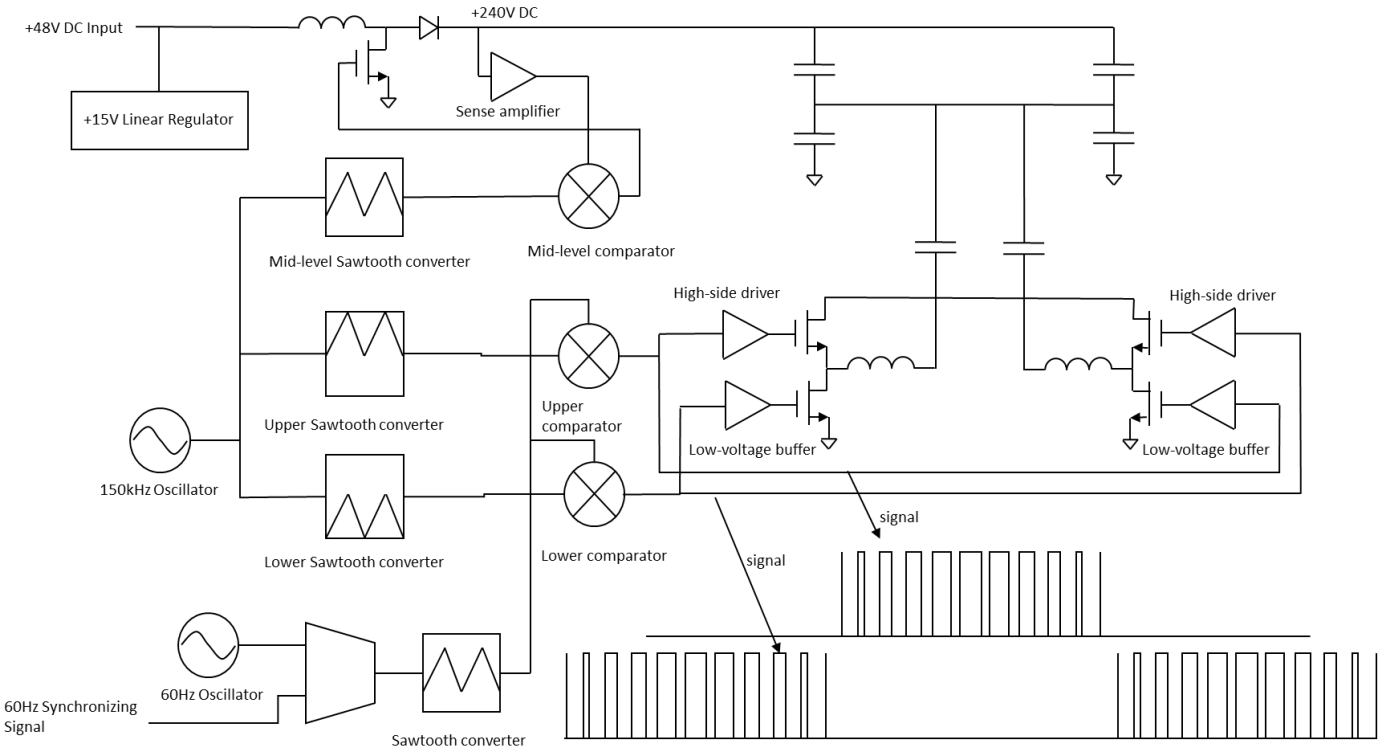


Figure 5: Boost Converter/ Inverter Detailed Functional Diagram